Experimental test of quasilinear theory

S. I. Tsunoda,[a] F. Doveil,[b] and J. H. Malmberg
Department of Physics, University of California, San Diego, La Jolla, California 92093

(Received 27 September 1990; accepted 24 June 1991)

The use of the random phase approximation in quasilinear theory has been controversial for some time. For the bump-on-tail instability this approximation leads to the neglect of mode coupling effects mediated by the resonant particles. Recently, it has been argued theoretically and numerically that resonant particle mediated mode coupling effects actually play an important role, and that the statistically averaged effect of this mode coupling is a zeroth-order increase in the growth rate. The quasilinear theory of the interaction between a warm beam and a slow wave structure is formally identical to the quasilinear theory of the interaction between a warm beam and a plasma in the weak beam limit. Strong mode coupling effects have been experimentally observed when a weak warm beam interacts with waves on a slow wave structure. When a statistical average is done over the mode coupling, however, the predicted zeroth-order increase in the growth rate is not observed.

I. INTRODUCTION

The prototypical example of the development of turbulence in plasmas is the interaction between a low-density, warm electron beam and a plasma (also known as the bump-on-tail instability). When a low-density, warm electron beam is injected into a plasma, a spectrum of modes may become unstable and grow at the expense of the beam kinetic energy. In the traditional quasilinear description[1] the mode growth rate is proportional to the slope of the time-averaged velocity distribution function evaluated at the phase velocity of the mode. As the waves grow, energy is extracted from the beam in such a way as to reduce the slope of the distribution function in the vicinity of the phase velocities of the waves. Saturation occurs when this slope is reduced to zero thus forming a plateau in the time-averaged velocity distribution function.

The principal simplifying assumption in quasilinear theory is the random phase approximation. This assumption, which leads to the neglect of mode coupling mediated by the beam, has been controversial for some time. Since the beam dynamics are highly nonlinear, one might expect that there would be contributions to the electric field of a mode due to nonlinear products of other modes. These contributions are neglected in the quasilinear description. Twenty years ago, a detailed experimental test of quasilinear theory was performed by Roberson and Gentle.[2] However, they were unable to directly check for the presence of mode coupling effects. The neglect of mode coupling effects has been criticized in the past using quite general theoretical arguments[3] and indeed, early computer simulation[4] showed some evidence for their existence. Recently, the neglect of beam mediated mode coupling has been shown to be suspect by explicit calculation.[5]

It has been further suggested[6] that when the mode coupling interactions are included in the theory, their statistically averaged effect is to cause a zeroth-order increase in the growth rates of the modes. It has been argued theoretically that as the beam electron orbits become nonlinear, the beam electrons begin to form clumps in phase space.[7] The clumps cause an enhanced drag force on the beam and thus produce an enhanced transfer of beam kinetic energy to wave energy, thereby increasing the growth rate. The growth rate has been predicted[6] to increase by about a factor of 2. In a recent computer simulation,[8] a zeroth-order increase in the wave growth rate has in fact been observed. However, in another, more recent computer simulation only a modest increase in the growth was observed.[9]

An important simplifying feature of the weak warm beam plasma instability is that if the beam is of sufficiently low density, then the background plasma behaves as a linear dielectric and acts only to support the waves.[10] We exploit this feature in our experiment by replacing the plasma with a slow wave structure. This replacement preserves the basic physics of the instability and, as we will show in this paper, in the weak beam limit, this ensures the mathematical correspondence between the interaction of a warm beam with a slow wave structure and the interaction of a warm beam with a plasma. Thus we inject a warm electron beam through a helical slow wave structure.[11]

This replacement of the plasma by a slow wave structure greatly reduces the background noise in the experiment. In fact, the background noise is sufficiently reduced that we can inject and thus control the spectrum of waves that interact with the beam particles. We have found our ability to define and control the input spectrum of waves to be crucial in our experimental study of this complex wave–particle interaction. In particular, we have been greatly aided by a technique that we have developed for use in this experiment—the use of repetitive "noise." By repetitive "noise," we mean an arbitrary but well-defined time-varying signal that lasts for some time, T, and that then repeats; T is generally chosen to be a time larger than the longest physically relevant time in the experiment. The use of repetitive noise allows us to study the

[a] Permanent address: General Atomics, P. O. Box 85608, San Diego, California 92186.
[b] Permanent address: Equipe Turbulence Plasma, Institut Méditerranéen de Technologie, 13451 Marseille, France.

 0899-8221/91/102747-11$02.00

actual dynamics of the turbulent wave–particle interaction. We may then perform well-defined statistical averages of our measured dynamical quantities.

We have observed strong mode coupling effects which are neglected in standard quasilinear theory. However, when we average over these mode coupling effects, we do not observe the predicted zeroth-order increase in the growth rate.

The paper has been organized as follows. In Sec. II we derive the quasilinear equations of the warm beam slow wave structure interaction and compare them to those of the warm beam plasma interaction. In Sec. III we describe the experimental apparatus. In Sec. IV we present our results and in Sec. V we state our conclusions.

II. THEORY

Here we derive the quasilinear equations of the warm beam slow wave structure interaction. We will show that in the weak beam limit, these equations are identical to the quasilinear equations[12] of the warm beam plasma interaction. When the beam is of small but finite strength, a correction term due to the beam space charge occurs in the quasilinear dispersion relation. We have shown in a previous paper[13] that in the weak beam limit the interaction between a weak cold beam and a single wave in a plasma is mathematically identical to the interaction between a weak cold beam and a single wave on a slow wave structure. Here we make a similar identification for the weak warm beam many-wave interaction.

The interaction between the beam electrons and the growing spectrum of waves is characterized by the ratio of the particle autocorrelation length to the spatial growth length, η_p, and by the ratio of the field autocorrelation length to the spatial growth length, η_s. We are interested in the case in which these ratios are less than unity. Here, η_p is inversely proportional to the spread in particle velocity in the beam, $\eta_p = k_i\omega/k^2\Delta v_p$, and η_s is inversely proportional to the spread in wave number in the spectrum,

$$\eta_s = \frac{k_i}{\Delta(k-\omega/v_\phi)} = \frac{k_i}{(1/v_g - 1/v_\phi)\Delta\omega}.$$

Here, v_g and v_ϕ are typical group and phase velocities of waves within the bandwidth, $\Delta\omega$, of the spectrum; ω, k, and k_i are the angular frequency, wave number, and spatial growth rate of a typical mode in the spectrum; Δv_p represents the width of the distribution function; in our experiment we define $\Delta v_p = v_{75} - v_{25}$, where v_{75} and v_{25} are the velocities at which the unperturbed beam parallel energy distribution function has decreased down its positive slope to 75% and 25% of its maximum value, respectively. In the experiment $0.038 < \eta_p < 0.098$ and $0.17 < \eta_s < 0.36$. In the following derivation, we assume $\eta_s,\ \eta_p \ll 1$.

We assume the beam dynamics to be one dimensional and use the one-dimensional Vlasov equation for the beam distribution, $f(r,z,v,t)$,

$$\frac{\partial f}{\partial t} + v\frac{\partial f}{\partial z} - \frac{e}{m}E_T\frac{\partial f}{\partial v} = 0. \tag{1}$$

We employ a cylindrical geometry: r and z are the radial and axial coordinates; v is the axial velocity, t is time, m is the electron mass, and $-e$ is the electron charge. We express the self-consistent, axial electric field, E_T, felt by the electrons as the sum of two parts—a part due to the waves on the slow wave structure, $E(r,z,t)$, and a part due to the beam space charge, $E_{SC}(r,z,t)$:

$$E_T(r,z,t) = E(r,z,t) + E_{SC}(r,z,t). \tag{2}$$

The principal difference between the beam plasma interaction and the beam slow wave structure interaction is that in the former system, $E_T(r,z,t)$ is given by Poisson's equation, while in the latter $E_{SC}(r,z,t)$ is given by Poisson's equation and $E(r,z,t)$ is given by an inhomogeneous wave equation.

We assume a discrete set of modes and we let

$$\begin{aligned} f(r,z,v,t) &= \frac{1}{2}\left(\sum_n f_{\omega_n}(r,z,v)e^{-i\omega_n t} + \text{c.c.}\right), \\ E_T(r,z,t) &= \frac{1}{2}\left(\sum_n E_{T_{\omega_n}}(r,z)e^{-i\omega_n t} + \text{c.c.}\right), \\ E(r,z,t) &= \frac{1}{2}\left(\sum_n E_{\omega_n}(r,z)e^{-i\omega_n t} + \text{c.c.}\right), \\ E_{SC}(r,z,t) &= \frac{1}{2}\left(\sum_n E_{SC_{\omega_n}}(r,z)e^{-i\omega_n t} + \text{c.c.}\right), \end{aligned} \tag{3}$$

where by "mode" we mean one of the terms in the above set of series. Since we have imposed periodicity in time the Fourier decomposition into discrete modes of frequency ω is mathematically correct. Whether or not this Fourier decomposition is the physically most transparent way to describe the problem is by no means obvious. However, for the purposes of following the traditional quasilinear description we will make the usual development in Fourier decomposed modes.

We obtain

$$\left(v\frac{\partial}{\partial z} - i\omega_n\right)f_{\omega_n} = \frac{e}{m}\sum_{\omega_{n'}} E_{T_{\omega_n-\omega_{n'}}}\frac{\partial f_{\omega_{n'}}}{\partial v}. \tag{4}$$

For $\omega_n = 0$

$$v\frac{\partial f_0}{\partial z} = \frac{e}{m}\sum_{\omega_{n'}} E_{T_{-\omega_{n'}}}\frac{\partial f_{\omega_{n'}}}{\partial v}. \tag{5}$$

We assume that the zero frequency components of the slow wave structure electric field and the beam space-charge electric field are zero; $E_0 = E_{SC_0} = 0$. For $\omega_n \neq 0$,

$$\left(v\frac{\partial}{\partial z} - i\omega_n\right)f_{\omega_n} - \frac{e}{m}E_{T_{\omega_n}}\frac{\partial f_0}{\partial v} = \frac{e}{m}{\sum_{\omega_{n'}}}' E_{T_{\omega_n-\omega_{n'}}}\frac{\partial f_{\omega_{n'}}}{\partial v}. \tag{6}$$

The prime on the sum indicates that the $\omega_{n'} = 0$ is not included. The right-hand side (rhs) represents mode coupling due to nonlinearities in the beam orbits. These nonlinearities couple frequency components of both the field of the mode on the slow wave structure, E_{ω_n}, and the field due to the beam space charge, $E_{SC_{\omega_n}}$. In the quasilinear approximation we neglect the terms on the rhs. In neglecting the rhs we are also neglecting the higher harmonics of the beam space-charge electric field. Please note that since we neglect the mode coupling terms, any subtle differences between mode coupling in a beam plasma system and a beam slow wave structure system are also neglected. Integrating over perturbed orbits,[14]

$$f_{\omega_n} = \frac{e}{m} \frac{E_{T_{\omega_n}}}{i(k_n v - \omega_n)} \frac{\partial f_0}{\partial v}, \tag{7}$$

where $k_n(\omega_n)$ is determined by the dispersion relation. Thus far we have followed the same formalism as in the beam plasma case.[12] Equation (7) is essentially Eq. (13) of Ref. 12. In the warm beam slow wave structure interaction we use an inhomogeneous wave equation instead of Poisson's equation to solve for E_{ω_n}. From the transmission line equations (see, for example, Ref. 11, p. 9), we have

$$\frac{\partial^2 V_{\omega_n}}{\partial z^2} + k_{0n}^2 V_{\omega_n} = R\omega_n k_{0n} \rho_{\omega_n}, \tag{8}$$

where

$$E_{\omega_n} = -\frac{\partial V_{\omega_n}}{\partial z},$$

$$\rho(r,z,t) = \frac{1}{2}\left(\sum_n \rho_{\omega_n}(r,z) e^{-i\omega_n t} + \text{c.c.}\right), \tag{9}$$

where $\rho(r,z,t)$ is the charge density of the beam and $k_{0n} = k_{0n_r} + ik_{0n_i}$ is the wave number in the absence of the beam. We assume that $k_{0n_i} \ll k_{0n_r}$. Here R is the interaction impedance of the slow wave structure and is given by

$$R(\omega_n) = \langle E_{\omega_n}^2 \rangle_b / 2k_{0n_r}^2 P_{\omega_n}, \tag{10}$$

where $\langle E_{\omega_n}^2 \rangle_b$ is the square of the slow wave structure electric field averaged over the area of the beam and P_{ω_n} is the power of the wave on the slow wave structure. The beam density is assumed to be uniform over its cross-sectional area. We obtain

$$E_{\omega_n} = [iR\omega_n k_{0n} k_n / (k_n^2 - k_{0n}^2)]\rho_{\omega_n}. \tag{11}$$

For the space-charge electric field, we use Poisson's equation. In cylindrical coordinates

$$\frac{\partial^2 V_{SC_{\omega_n}}}{\partial r^2} + \frac{1}{r}\frac{\partial V_{SC_{\omega_n}}}{\partial r} - k^2 V_{SC_{\omega_n}} = -4\pi\rho_{\omega_n}, \tag{12}$$

where

$$E_{SC_{\omega_n}} = -\frac{\partial V_{SC_{\omega_n}}}{\partial z}. \tag{13}$$

For the purpose of calculating $E_{SC_{\omega_n}}$, we model the helical slow wave structure as a conducting cylinder. This has proven to be a good model[15] in the cold beam case. Then near the helix axis,

$$E_{SC_{\omega_n}} = \frac{4\pi\rho_{\omega_n}}{ik_n} P_q = \frac{-4\pi P_q e n_b}{ik_n} \int f_{\omega_n}\, dv, \tag{14}$$

where n_b is the beam density. Here P_q is the plasma frequency reduction factor. Branch and Mihran[16] have tabulated values of P_q for many beam geometries including the case in which a constant density beam partially fills the cylinder. Using Eqs. (2), (7), and (14),

$$\frac{E_{SC_{\omega_n}}}{E_{\omega_n}} = \frac{(\omega_q^2/k_n)\int[\partial f_0/\partial v/(k_n v - \omega)]\,dv}{1 - (\omega_q^2/k_n)\int[\partial f_0/\partial v/(k_n v - \omega_n)]\,dv} \equiv H_q, \tag{15}$$

where we define $\omega_q^2 = P_q \omega_b^2$ where ω_b is the beam plasma frequency. Combining Eqs. (7), (11), and (15) we have

$$1 = -\frac{R\omega_n k_{0n} k_n(z) e^2 n_b}{[k_n^2(z) - k_{0n}^2]m}[1 + H_q(z)] \times \int \frac{\partial f_0(z)/\partial v}{k_n(z)v - \omega_n} dv. \tag{16}$$

In the weak beam limit $H_q \to 0$. We assume $(k_n - k_{0n})/k_{0n}$ is small and to lowest order in this quantity,

$$\frac{k_n - k_{0n}}{k_{0n}} = -\frac{I_0 R}{4V_0} u_0 \frac{\omega_n}{k_{0n}} \left(\fint \frac{\partial f_0(z)/\partial v}{v - \omega_n/k_n} dv + i\pi \frac{\partial f_0(z)}{\partial v}\bigg|_{v=\omega_n/k_{0n}} \right), \tag{17}$$

where I_0 is the beam current, V_0 is the cathode voltage, u_0 is a velocity satisfying $I_0 = n_b e u_0$ and $eV_0 = \frac{1}{2}mu_0^2$, and $\fint$ denotes the principal value of the integral.

We note that if we equate

$$\frac{I_0 R}{4V_0} = -\frac{\omega_p^2}{\omega_n^2}\frac{n_b}{n_0}\frac{1}{(u_0/\omega_n)k_n^2(\partial\epsilon/\partial k)_{\omega_n, k_{0n}}}, \tag{18}$$

we recover the beam plasma quasilinear expression for spatial wave growth. Here n_0 is the plasma density, ω_p is the plasma frequency, and ϵ is the linear plasma dielectric function. This is the same equality that is made in order to formally identify[13] the small cold beam plasma equations[17] with the nonlinear traveling wave tube equations.[18]

In order to obtain the diffusion equation, we combine Eqs. (5) and (7)

$$v\frac{\partial f_0}{\partial z} = \frac{\partial}{\partial v} D(z,v) \frac{\partial f_0}{\partial v}, \tag{19}$$

$$D(z,v) = \frac{e^2}{m^2} \sum_n \frac{|E_{T_n}|^2}{i(k_n v - \omega_n)}. \tag{20}$$

This expression is formally the same as Eq. (17) in Ref. 12.

Thus, we see that in the weak beam limit ($H_q \to 0$) the quasilinear equations of the weak warm beam slow wave structure system are formally identical to those of the weak warm beam plasma system. When H_q is nonzero, a correction term occurs in the quasilinear dispersion relation. In the experiment, we estimate $-0.08 < \text{Re}\, H_q < -0.05$ and $0.07 < \text{Im}\, H_q < 0.1$ for harmonic beam perturbations.

III. EXPERIMENTAL APPARATUS

The apparatus, which has been described in detail elsewhere,[13,19] is shown schematically in Fig. 1. In essence it is a traveling wave tube[11] modified so that a warm beam rather than a cold beam interacts with the waves on the slow wave structure.

The electron beam is directed along the axis of a helical slow wave structure and is confined by a strong (Larmor frequency is large compared to all other frequencies) axial magnetic field ($B_z = 440$ G). The electron source is a standard tungsten dispenser cathode of radius 0.38 cm. A cold electron beam is formed with a Pierce-type structure consisting of the cathode, the forming electrode, and the anode. This cold beam is made warm by passing it through three parallel, closely spaced, wire mesh grids. The two outer grids

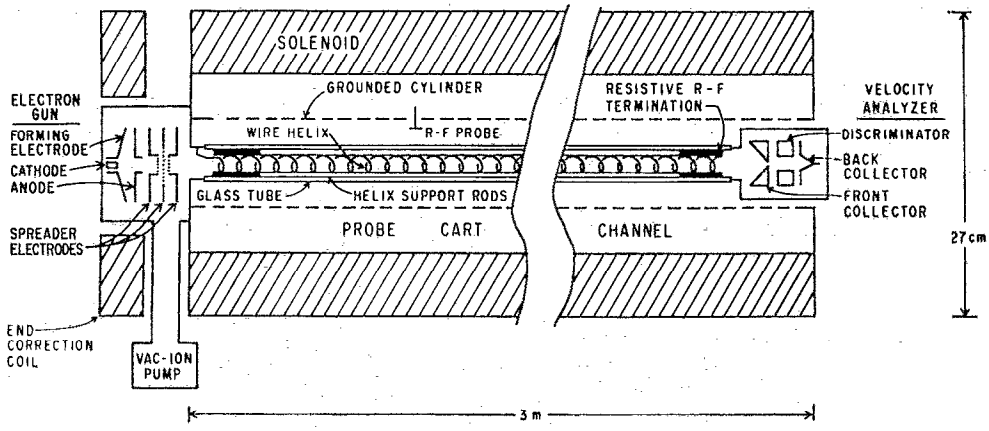

FIG. 1. Schematic diagram of the apparatus (not drawn to scale).

are grounded and the middle grid is biased at a high positive potential V_s. Because of the strong electric fields near the grid wires, some of the axial kinetic energy of the electrons is scattered into perpendicular kinetic energy. Thus, by adjusting V_s we can control the axial velocity spread of the beam. Of course, since the total kinetic energy of each electron is conserved in this process, there is a corresponding perpendicular velocity spread of the beam. The cyclotron motion of the particles does not affect the behavior of the waves on the slow wave structure since the cyclotron frequency is 1.2 GHz, which is much too high to couple efficiently to the slow wave structure. The beam radius is 0.34 cm.

The electron beam is pulsed by applying a square gating pulse to the anode. The beam electrons produce ions through their collisions with the residual background gas. The base pressure is 1×10^{-6} in the middle of the tube. We pulse the beam in order to prevent the ions from accumulating. A large ion population in the tube would give rise to ion noise which would produce undesirable effects. The time duration of the current pulse is typically 400 μsec. The pulse repetition rate is 60 Hz. Thus a pulsed electron beam with a controllable axial velocity spread is directed along the axis of the slow wave structure.

The slow wave structure is a wire helix that is rigidly held together by an insulating support structure and is enclosed by a glass vacuum tube. A resistive rf termination at each end of the helix serves to reduce reflections. Reflected waves originate from slight irregularities in the radius and pitch of the helix as well as from the ends. The maximum voltage standing wave ratio is 1.26. Since the backward wave is far from synchronism with the beam, the effect of the backward wave on the beam dynamics is negligible. The helix assembly is enclosed by a glass vacuum jacket which in turn is enclosed by an axially slotted 3.8 cm radius cylinder that defines the rf ground. Inside the cylinder but outside the vacuum jacket are four axially movable rf probes. The probes couple capacitively to the helix. The cylinder, which has a cutoff frequency of 3.0 GHz, is a waveguide beyond cutoff for the frequencies used in the experiment. This ensures that for these frequencies, the only traveling waves that can exist in the tube propagate on the helix.

Most of the beam is collected immediately after passing through the helix. A small fraction of the beam passes through a hole in the collecting electrode, then through the discriminator tube, and then separately collected. By biasing the discriminator tube and measuring the current that gets through it, we can determine[20] the time-averaged parallel velocity distribution function of the beam.

The receiver consists of a probe followed by a step attenuator, a low-noise amplifier, and a spectrum analyzer. The output of the spectrum analyzer is sampled and held. The held output is applied to the Y channel of an X-Y recorder. A voltage proportional to the axial position of the probe is applied to the X channel of the X-Y recorder. The probe is moved along the helix and thereby plots of wave power at a particular frequency versus axial distance are produced. For many of the plots shown in this paper we employ two probes configured as a directional coupler. This is done to reduce the backward wave component of the signal. The two probes move together but are separated by distance $\lambda/4$ where λ is the wavelength of the mode we wish to measure. The signal received by the upstream probe is delayed in time by $1/4f$ where f is the frequency of the mode. The vector sum of the signals from these two probes is a constructive interference of the components traveling downstream received by each probe and a destructive interference of the two backward components.

Figure 2 is a plot of the dispersion of the helical slow wave structure. The dispersion relation closely resembles that of a finite radius, finite temperature plasma.[21] There is an experimental advantage to using a slow wave structure rather than a plasma to support the wave propagation. Unlike a plasma, the helix does not introduce any appreciably noise. In a beam plasma system, low-frequency ion noise causes phase jitter in the unstable spectrum which makes mode coupling measurements very difficult. By replacing the plasma with a slow wave structure we eliminate these undesirable effects.

Because the background noise level in our experiment is very low, we are in a position to define and control the input wave spectrum. A particularly interesting way to do this is to launch repetitive "noise." By repetitive "noise" we mean an arbitrary but well-defined time-varying signal that lasts for some time T, and that then repeats. This time-varying signal could, for example, be a sample of duration T taken from truly random noise such as bandlimited Johnson noise. Gen-

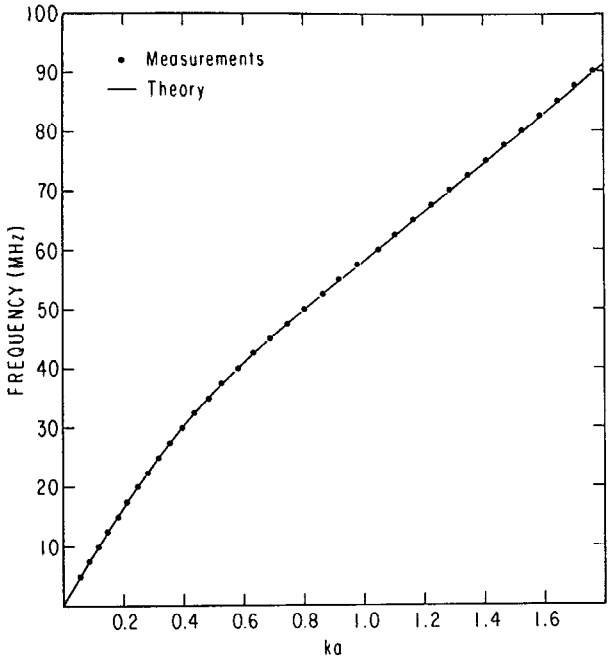

FIG. 2. Dispersion relation for the slow wave structure. The points are the measured results, and the line is the result of calculation; $a = 1.08$ cm is the helix radius.

erally, T is chosen to be a time longer than the longest physically relevant time in an experiment. In our case, this is the beam transit time ($\sim 0.5\,\mu$sec).

We manufacture this repetitive "noise" using a computer controlled, high-speed arbitrary waveform generator that was built for this purpose and which has been described in detail elsewhere.[22] This device allows us to prescribe the complex Fourier coefficient of each mode of the launched spectrum.

There are substantial advantages to using repetitive "noise." The use of repetitive "noise" enables us to study our turbulent system with all relevant initial conditions under our control and with all genuine randomness eliminated from the dynamical variables that describe the system. In many experiments that study turbulence, one is unfortunately only able to measure statistical quantities. In our experiment, the ability to launch repetitive noise enables us to study the dynamics of this complex wave–particle interaction. If we desire, we may subsequently perform well-defined statistical averages of the dynamical quantities that we measure.

Because the waveform repeats, it is possible to follow the evolution of a launched waveform with a single receiving probe that is slowly moved down the tube. One could accomplish the same thing with a multiplicity of receiving probes positioned along the tube with each probe recording the time variation of nonrepetitive noise for a sufficiently long time duration (say, two or three beam transit times). The evolution of a given time segment of the nonrepetitive noise could then be pieced together from the individual temporal waveforms recorded at each successive probe position. This approach would be quite unwieldy in practice due to the number of probes and recording devices required. It has the additional disadvantage that each experiment is irreproducible. Using a repetitive waveform only a single, movable, receiving probe is required. Moreover, if it can be continuously moved, the evolution of the noise can be determined to arbitrary spatial resolution.[23] Also, each experiment is reproducible. As far as the interaction with the beam electrons is concerned, repetitive "noise" is indistinguishable from nonrepetitive noise so long as the repetition time of the noise is sufficiently long (longer than the beam transit time).

The use of repetitive "noise" also enables one to *define* the launched waveform with which the electrons interact at the beginning of the tube. This means, for example, that we can compare the evolution of a given launched spectrum whose complex Fourier components we control, with that of a launched spectrum that is different in some manner and determine how the interaction depends on the difference. The use of repetitive "noise" therefore gives us a powerful means for investigating the complex wave–particle interaction.

Figure 3 is a plot of the interaction impedance, R, versus ka, where $a = 1.077$ cm is the helix radius (measured from the helix axis to the wire center). The solid line in Fig. 3 is calculated using Eq. (10) and using the known radial eigenfunctions for the electric field, E_{ω_n}, and the magnetic field, H_{ω_n}, for the helix in the absence of the beam.[11] The measured points are made using the Kompfner dip method which has previously been described in detail elsewhere.[19] This figure essentially gives the wave-number dependence of the left-hand side of Eq. (18). One difference between our slow wave structure and a cold infinite plasma is that for a cold infinite plasma the right-hand side of Eq. (18) is essentially independent of wave number.

Another advantage of the beam slow wave structure system is that the background noise level is so low that it is possible to measure the growth rate of a single wave launched far below saturation so that the time-averaged distribution function is essentially unchanged. This single wave growth rate is very useful. Since it is the only wave in the system, no mode coupling is possible, and it is thus an experi-

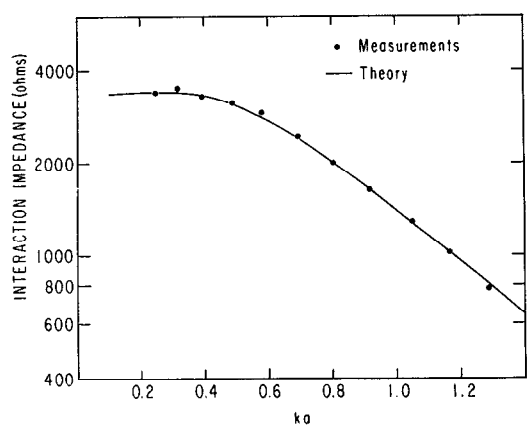

FIG. 3. Interaction impedance of the slow wave structure. The points are the measured results, and the line is the result of calculation.

mental definition of the Landau growth rate. In Fig. 4 we show a plot of the single wave corrected growth rate as a function of beam density. The corrected growth rate is obtained by subtracting the measured helix damping rate from the measured growth rate. The density is varied by increasing the beam current and keeping the beam voltage the same. The dots represent the measured growth rates and the line is the theoretical prediction given by the Landau formula [Eq. (17)] and the slope of the measured time-average distribution function of the beam.

IV. RESULTS

A. Saturation and plateau formation

We have observed the growth and saturation of broadband noise in the warm beam slow wave structure system. The background noise level is sufficiently low that in the absence of any launched waves, all wave activity is far below the saturation level of the instability. We launch the noise in our experiment by applying an rf voltage to a probe near the gun end of the machine. For example, we may launch broadband noise that has been derived from the input noise of an amplifier. In Fig. 5(a) we show a plot of the logarithm of the total received power as a function of axial distance down the tube. The wave power is seen to grow exponentially nearly 15 dB and then saturate. In Fig. 5(b) we show the corresponding evolution of the time-averaged parallel energy distribution function of the beam. The position of the retarding field analyzer used to measure it is fixed at the downstream end of the machine and cannot be moved upstream to observe the early evolution of the beam. However, when we move the transmitting probe to another z position, the wave power as a function of axial distance is axially translated with the transmitting probe. So by moving the probe closer to the downstream end, we bring to that end an earlier point in the evolution of the noise and the beam. Figure 5(b) shows the evolution of the distribution function measured in this way. As the noise grows and saturates, the beam distribution is seen to evolve into a plateau.[24]

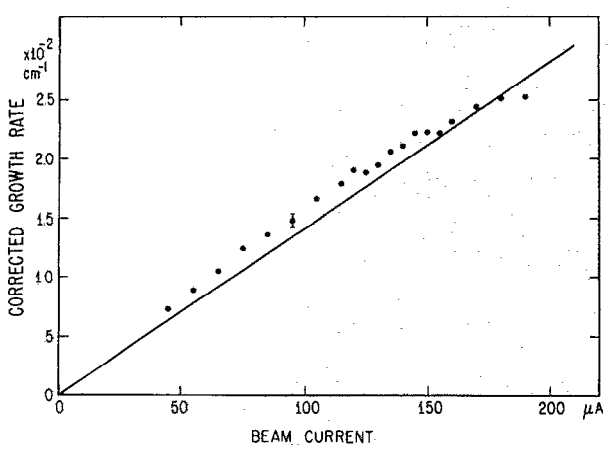

FIG. 4. Corrected single wave growth rate, $k_i - k_{0i}$, versus beam current with the beam voltage held fixed; $V_0 = 65$ V, $V_s = 2$ kV, $f = 65$ MHz.

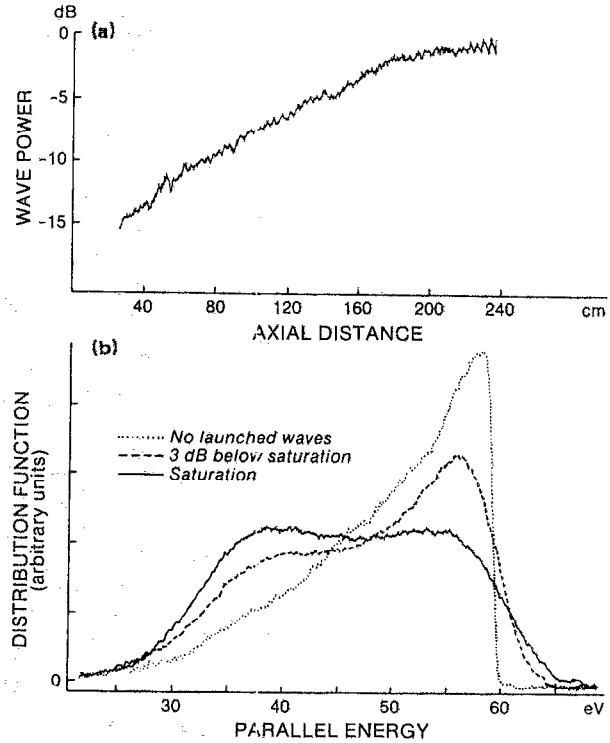

FIG. 5. (a) Total wave power versus axial distance. Beam voltage, $V_0 = 60.0$ V; $I_0 = 110$ μA; spreader bias voltage, $V_s = 2.0$ kV, $\eta_p = 0.065$, $\eta_s = 0.17$. (b) Time-averaged beam parallel energy distribution function at various positions versus parallel energy. Same parameters as (a). The launch level is held constant.

The observation of a smooth plateau together with the good agreement between the measured single wave growth rate and the Landau warm beam expression are good indications that the values of η_s and η_p are sufficiently small in our device for the predictions of quasilinear theory to apply. Although the best way to check that our values for η_s and η_p are sufficiently small is to carry out quasilinear theory to second order in these quantities, we have not done this. It is well known,[25] however, that there is a smooth transition between the behavior of the weak warm beam plasma system and the weak cold beam plasma system as η_s and η_p are varied. There is a mathematically identical transition in the weak beam slow wave structure case. The beginning[2] of the transition from warm beam behavior to cold beam behavior is marked by the emergence of structure on the time-averaged velocity distribution function corresponding to trapped particle formation. This does not appear in Fig. 5(b). In addition, in the cold beam case the linear growth rate is proportional to $I_0^{1/3}$ whereas in the warm beam case it is linearly proportional to I_0. Figure 4 clearly shows a linear dependence on I_0.

B. Existence of strong coupling effects

With the aid of the arbitrary waveform generator we have observed strong mode coupling effects. Figure 6(a) shows a typical launched spectrum of repetitive "noise." The

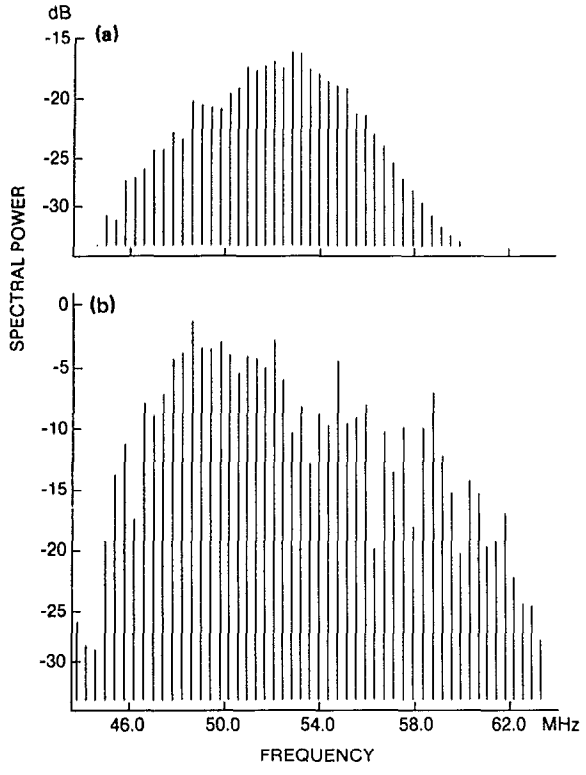

FIG. 6. (a) Spectrum launched by the arbitrary waveform generator. The spectral lines shown here and in (b) and Fig. 7(a) are meant to show only the measured power at each mode frequency. The finite linewidth at each frequency has been suppressed for clarity. (b) Spectrum downstream; $V_0 = 60.0$ V, $I_0 = 140\,\mu$A, $V_s = 2.5$ kV, $\eta_p = 0.098$, $\eta_s = 0.36$.

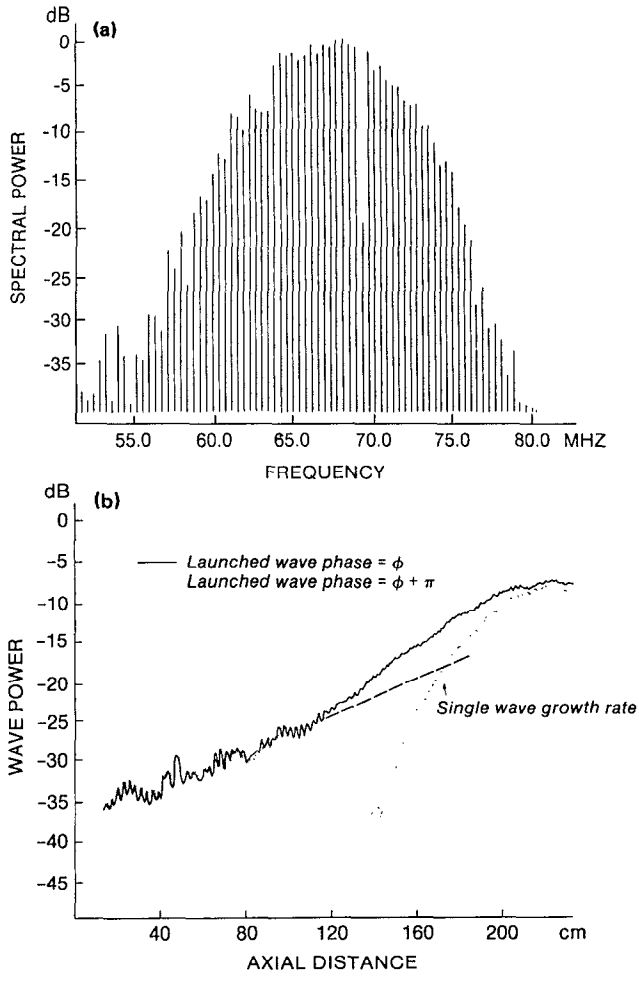

FIG. 7. (a) Spectrum used to further investigate the mode coupling. (b) Wave power versus axial distance of the small mode with phase $= \phi$ (solid curve) and of the mode with phase $= \phi + \pi$ (dotted curve). Here $V_0 = 60.0$ V, $I_0 = 110\ \mu$A, $V_s = 2.0$ kV, frequency, $f = 69.12$ MHz; $\eta_p = 0.038$, $\eta_s = 0.20$.

amplitudes of the modes (which are discrete[26] since the signal is repetitive with period $= 2.56\,\mu$sec) have been chosen to be a smooth function of frequency, but their phases have been chosen by a random number generator in the computer. Figure 6(a) shows the spectrum measured upstream, near the transmitter. Figure 6(b) shows the spectrum downstream. The modes have grown due to their interaction with the beam and most of them saturated. However, their amplitudes are no longer the smooth function of frequency predicted by standard quasilinear theory. As the time-averaged distribution function evolves, quasilinear theory predicts that it remains a smooth function of velocity. We, in fact, observe this to be the case in our experiment [as shown in Fig. 5(b)]. However, since quasilinear theory also assumes that the growth depends only on the time-averaged part of the distribution function, it therefore predicts that the spectrum, if originally smooth, should remain smooth throughout the entire nonlinear evolution up to saturation. We see from Fig. 6(b) that this is not the case experimentally. This nonsmooth behavior has also been seen in computer simulations.[4,8,9]

The nature of this behavior was investigated further by launching a spectrum which was similar to that of Fig. 6(a) but with one of the modes near the middle of the spectrum having a level 20 dB below the neighboring modes. This spectrum is shown in Fig. 7(a). The solid line in Fig. 7(b) shows how this mode evolves as a function of axial distance down the tube. Up to $z = 100$ cm the mode grows at the single wave growth rate. The single wave growth rate was determined by replacing the arbitrary waveform generator with a signal generator set to the frequency of the mode. The growth rate of this single wave is represented by the dashed line in Fig. 7(b). As mentioned above, this single wave growth rate is our experimental definition of the Landau growth rate. At $z = 100$ cm the wave exhibits a change in growth rate and continues to grow at an enhanced growth rate until it saturates. The dotted curve shows the evolution when we change the phase of the small launched mode by 180° and leave the phases and amplitudes of all the other modes the same. Again the mode grows at the single wave growth rate until about 90 cm, where, in this case, it experiences a dramatic dip in power. It then grows at an enhanced growth rate until it saturates.

This behavior is due to mode coupling into this frequency caused by the surrounding larger modes. The electric field

received by the probe at this frequency consists of two contributions. One contribution comes from the launched mode. The other is due to surrounding larger modes which couple together and produce an induced electric field at this frequency. In the case of the solid curve in Fig. 7(b), these contributions are combining constructively. In the case of the dotted curve they are combining destructively. The solid and dotted curves in Fig. 7(b) were selected to show the extreme cases of this effect. For values of the phase of the small launched wave intermediate between ϕ and $\phi + \pi$, the corresponding curve is observed to have an intermediate behavior between the solid and dashed curves. For a smooth sequence of phases from ϕ to $\phi + \pi$ we observe a sequence of curves representing a smooth variation of behavior from that shown by the solid curve to that shown by the dotted curve.

The fast oscillations seen in this plot are due to a beat between the forward wave and a small component of backward wave originating from reflections from the end of the helix and from irregularities in the windings. Since the backward wave is far out of synchronism with the beam, its interaction with the beam is negligible. The fast oscillations have been reduced (but not eliminated) by using the two-probe directional coupler technique [in both Figs. 7(b) and 8]. In addition, there are very weak slow oscillations visible in the plot, especially in the region between 40 and 100 cm. These are due to a beat between the forward wave on the helix and a passive mode on the beam. We regard these small amplitude oscillations as incidental to the main effect shown in Fig. 7, namely, that the mode coupling can cause dramatic effects on the evolution of the modes.

C. Measurements of the average growth rate

When we average over these mode coupling effects we do not observe the predicted zeroth-order increase in the growth rate. At each axial position along the helix the square of the electric field is averaged. Three different kinds of averaging procedures have been tried. The different averaging methods (to be discussed below) are characterized by what is varied when the average is taken. We then determine the spatial growth rate of the average. None of these averaging methods result in a zeroth-order increase in the growth rate.

One type of averaging is ensemble averaging. The waveform generator is used to launch repetitive "noise" corresponding to a set of randomly chosen initial amplitudes and phases. We average the square of the electric field of a mode from this noise over different sets of randomly chosen initial amplitudes and phases.

Another averaging method is frequency averaging. Again the waveform generator is used to launch repetitive "noise." In this case, we average the square of the electric fields of a number of modes within the receiver bandwidth. Here we use a single set of randomly chosen initial amplitudes and phases. Ensemble averaging and frequency averaging are equivalent in the limit of infinitely many modes if the bandwidth over which we frequency average is much smaller than the reciprocal of the longest physically relevant time scale. We assume this to be the beam transit time.

We have also performed combined frequency and ensemble averaging. This is done by replacing the waveform generator with a nonrepetitive noise source (the input noise of an amplifier). A frequency average of the square of the electric field is taken over the receiver bandwidth. This frequency average is in turn averaged over time. These three averaging techniques will be described in further detail below. We first present our results from the combined frequency and ensemble average.

The combined frequency and ensemble average over the mode coupling effects does not result in the predicted zeroth-order increase in the growth rate. To demonstrate this we first launch a smooth spectrum of modes using the arbitrary waveform generator [similar to the spectrum of Fig. 6(a)]. The dashed line in Fig. 8 shows the evolution of one of the modes. Strong mode coupling effects are seen to occur beginning at $z = 80$ cm. If we launch a single mode at low amplitude, we obtain our experimental definition of the Landau growth rate. This is shown in Fig. 8 by the dotted curve. Next we replace the waveform generator with a nonrepetitive noise source. The nonrepetitive noise is similar to the waveform generator noise in both shape and magnitude. We receive with a narrow-band receiver (bandwidth = 100 kHz) that squares the received electric field and then time averages it (averaging time > 100 μsec). Thus, during each beam pulse, a frequency average over the receiver bandwidth is taken. These frequency-averaged values are then ensemble averaged over many beam pulses. The solid curve shows the evolution of the logarithm of this average. To good accuracy (better than 10%) no deviation from the Landau growth rate is seen.

It is possible that a change in the average growth rate due to mode coupling could be masked by an opposing change in the slope of the time-averaged distribution function. So, to further ensure the validity of this result we show below that at the onset of the strong mode coupling near $z = 80$ cm, no substantial change has occurred in the time-averaged distribution function. The saturation level for the case shown in Fig. 8 is around 0 dB on the plot. The onset of

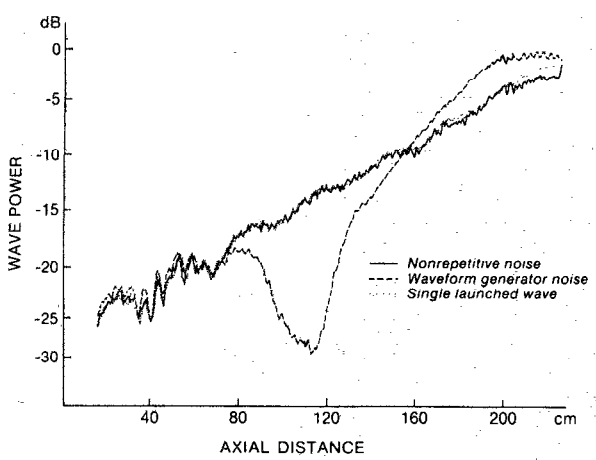

FIG. 8. Wave power versus axial distance for various launched signals: Repetitive "noise" (dashed), nonrepetitive noise (solid), and a single wave (dotted). Here $V_0 = 60.0$ V, $I_0 = 140$ μA, $V_s = 2.5$ kV, $f = 62.34$ MHz; $\eta_p = 0.055$, $\eta_s = 0.19$.

the mode coupling occurs when the solid curve is between 15 to 20 dB below saturation. Figure 9 shows the time-averaged distribution function corresponding to various points in the growing level of the nonrepetitive noise. The curve labeled "10 dB below saturation," for example, corresponds to the time-averaged distribution function at the point where the solid curve in Fig. 8 is 10 dB below saturation. This could correspond to the time-averaged distribution function at $z = 140$ cm in Fig. 8. In Fig. 8 we see that the mode coupling is occurring around $z = 100$ corresponding to a power level 15 dB below saturation. In Fig. 9 it is seen that in the vicinity of the phase velocity of the wave (indicated by the arrow), the curves labeled "15 dB below saturation" and "no launched waves" overlay. Thus, no substantial change in the slope of the time-averaged distribution function has occurred during the onset of the mode coupling.

Although the analytic theories have predicted a growth rate enhancement of about a factor of 2 for all modes in the spectrum, computer simulations[8] have found that the growth rate enhancement should be even more dramatic near the edges of the spectrum. In the experimental case described above, the narrow band of noise we follow occurs near the high-frequency edge of the spectrum. We have similarly looked at the growth of a narrow band of noise near the low-frequency edge of the spectrum and at the growth of narrow bands of noise in the middle of the spectrum. Again we find, to good accuracy, no deviation from the Landau growth rate.

In the averaging experiment just described nonrepetitive noise was used to obtain a frequency and ensemble average. We may also construct a frequency average using the repetitive noise of the waveform generator. This is done simply by selecting a receiver bandwidth wide enough to include several noise generator modes (typically 3–10). The repetitive electric field within this bandwidth is squared and then time averaged. For any given averaging experiment only a single set of initial amplitudes and phases is used. Typically, the amplitudes and phases of the modes are chosen randomly using the random number generator in the computer. Since the noise is repetitive, the same signal occurs during each beam pulse and so no significant ensemble averaging is occurring. The logarithm of this average is compared with the growth of a single wave. No substantial deviation from the Landau growth rate is observed.

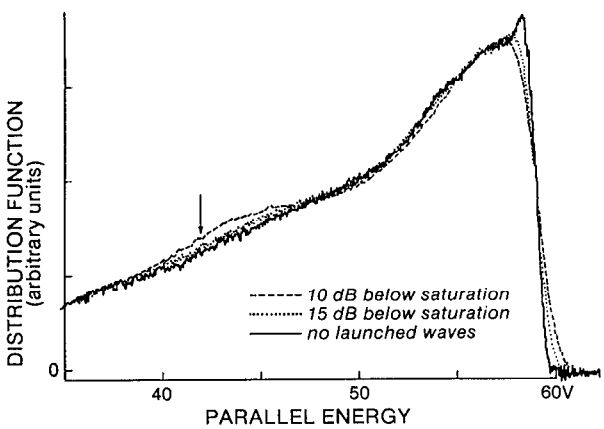

FIG. 9. Time-averaged beam parallel energy distribution function at various positions versus parallel energy. Same parameters as Fig. 8. The launch level is held constant.

The above method of averaging can be considered as pure frequency averaging with no significant concomitant ensemble averaging. We have also constructed pure ensemble averaging. To do this we transmit waveform generator noise as before, but we now receive the repetitive noise with a fast digitizer. By Fourier analyzing this signal, we have access to the complex Fourier coefficient of each mode at every axial position down the tube. For the purposes of averaging, however, we form the square of the modulus of the complex amplitude of a given mode and store its variation as a function of axial distance. We then select another sample of repetitive noise by choosing another random set of amplitudes and phases. We again form the square modulus of the mode and add its value to the stored value previously taken at each corresponding axial position. We repeat the process many times and then form the ensemble average. After averaging a sufficient number of samples (typically 8–16) the logarithm is taken and compared with the single wave growth. Again, no substantial deviation from the Landau growth rate is observed.

Thus we have investigated pure ensemble averaging, pure frequency averaging, and combined frequency and ensemble averaging. In no case do we observe any significant deviation from the Landau growth rate.

Another interesting experiment which is related to the above averaging experiments involves using the arbitrary waveform generator and a separate signal generator. Repetitive noise from the arbitrary waveform generator is launched together with a low-level sine wave from a separate signal generator. The frequency of the sine wave is in between two adjacent waveform generator frequency components. This sine wave always grows at the Landau growth rate. We show below that this result suggests that there is no significant trapped particle sideband instability[27] occurring in the experiment.

Let us first consider the character of the waveform generator signal above, in the absence of the separate signal generator. The repetition time of the waveform generator is determined by a single high-frequency clock and thus each frequency component generated by the device is a harmonic of a single frequency, the inverse repetition rate. In other words, every frequency component is of the form $f_n = n\Delta f$ where n is an integer and Δf is the inverse repetition rate. A necessary condition for mode coupling to occur among any m frequency components $f_1 f_2 \ldots f_m$ is the existence of time-independent whole numbers $n_1, n_2, \ldots, n_m$ such that $n_1 f_1 + n_2 f_2 + \cdots + n_m f_m = 0$. This is satisfied for the f_n of the form $f_n = n\Delta f$. Furthermore, the f_n's form a closed system. That is, mode coupling among f_n's of the form $f_n = n\Delta f$ can never create an $f_s = s\Delta f$ where s is not a time-independent integer. Let us now launch repetitive noise and in addition launch a low-level signal from a separate sine wave generator. The sine wave of frequency f_s is asynchro-

nous relative to the clock of the arbitrary waveform generated and thus $f_s = s\Delta f$ where s is not a time-independent integer.

Let us now consider adding the sine wave of frequency f_s from the separate signal generator. We know that the f_n's from the arbitrary waveform generator cannot by themselves couple and produce an electric field at f_s. However, it is possible that the signal at f_s could become *unstable* due to the perturbation produced in the beam from the repetitive noise. In the simplest case, a three-wave interaction between f_n, f_s, and $2f_n - f_s$ may occur. The signals at f_s and at $2f_n - f_s$ are small compared to the signal at f_n. The modes f_n and f_s are asynchronous in the sense previously described. This process was studied in connection with trapping by Kruer *et al.*[27] A large amplitude wave is launched at f_L in a cold beam plasma system which sets up an oscillating trapped particle distribution. Sidebands at f_s and $2f_L - f_s$ can become unstable. The unstable sideband at f_s is asynchronous to the launched wave f_L in the sense previously described. In fact, there is a continuous band of unstable upper and lower sideband frequencies. In our many-wave experiment, we envision the possibility that one or more of the waveform generator modes creates some oscillating trapped particles. It might then be possible for an asynchronous sideband at f_s to become unstable. The fact that this asynchronous frequency component grows at the Landau growth rate in our experiment suggests that there is no significant trapped particle sideband instability of the Kruer *et al.* type occurring in the experiment.

V. CONCLUSIONS

We have observed strong mode coupling effects when a weak warm beam interacts with waves on a slow wave structure. However, when we statistically average over these mode coupling effects, we do not observe a zeroth-order increase in the growth rate.

The observation of strong mode coupling effects means that quasilinear theory as applied to the warm beam slow wave structure system is incomplete. One cannot *a priori* neglect mode coupling terms in the theory. The absence of any zeroth-order increase in the growth rate when we average over the mode coupling in our system suggests the action of some statistical or dynamical conservation law whose origin has not yet been identified. The results that we have obtained may have important consequences for the understanding of the beam plasma instability as studied in laboratory plasmas, theoretical model calculations, and particle simulations.

We believe that the essential physics of the interaction between a weak warm beam and the waves in a plasma is the same as that of the interaction between a weak warm beam and the waves on a slow wave structure. In particular, we have shown that the quasilinear theories of these two systems are mathematically identical in the weak beam limit. The close relationship between our system and the spatially growing, finite-sized beam plasma system strongly suggests that our results can be carried over to the analogous laboratory plasma system.

Theories and computer simulations of the beam plasma interaction generally model the plasma as having infinite extent and impose periodic boundary conditions. That is, they consider the temporally growing instability of an infinite beam and plasma. Although compared to the analogous laboratory plasma system these theoretical models are still further removed from our experimental system, we suspect that in these models as well the essential physics is the same. If these theoretical and computational systems do differ from ours in a crucial way, the differences might be in the way the space-charge harmonic fields behave in an infinite, temporally growing beam plasma system as opposed to our finite, spatially growing beam slow wave structure system. Or, there may be some subtle difference in the nature of the mode coupling between the two systems.

If we can presume that the essential physics between our experiment and the theoretical models is the same, then we can make the following comments on recent theoretical developments. First, our results are in agreement with the assertion that quasilinear theory is not complete since we clearly observe mode coupling effects which are neglected in the quasilinear approximation. However, our results do not support the theoretical prediction of a zeroth-order increase in the statistically averaged growth rate.

Similar comments apply to recent computer simulation studies of the warm beam plasma system. Again, the computer simulations produced thus far model the interaction as a temporally growing one of infinite extent. As in our experiment, two prior computer simulations have observed strong mode coupling effects. One[8] also showed clear evidence of a zeroth-order increase in the average growth rate contrary to our experimental result. The other,[9] more recent simulation showed a more modest increase in the average growth rate. This simulation result is also contrary to our result as their observed increase in the average growth rate is greater than the limit imposed by the accuracy of our measurement.

To sum up, we have shown that the quasilinear description of our experiment is incomplete. The correct nonlinear description of our experiment has yet to be found. An important clue may be the existence of a statistical or dynamical conservation law governing the mode coupling effects. We believe these conclusions may also apply to analogous laboratory plasma systems, plasma theories, and particle simulations.

ACKNOWLEDGMENTS

We wish to thank Guy Laval, Tom O'Neil, and Denis Pesme for stimulating conversations. In addition we would like to thank Roy Gould for a careful reading of the manuscript. One of the authors (F.D.) gratefully acknowledges the hospitality of the Department of Physics of the University of California, San Diego, where this work was performed.

This work was supported by the National Science Foundation under Grants No. PHY83-06077 and No. PHY87-06358.

[1] W. E. Drummond and D. Pines, Nucl. Fusion, Suppl. Pt. 3, 1049 (1962); A. A. Vedenov, E. P. Velikhov, and R. Z. Sagdeev, Nucl. Fusion **1**, 82 (1961).

[2] C. Roberson and K. W. Gentle, Phys. Fluids **14**, 2462 (1971).

[3] T. M. O'Neil, Phys. Fluids **17**, 2249 (1974).
[4] D. Biskamp and H. Welter, Nucl. Fusion **12**, 89 (1983).
[5] G. Laval and D. Pesme, Phys. Fluids **26**, 52 (1983).
[6] G. Laval and D. Pesme, Phys. Rev. Lett. **53**, 270 (1984).
[7] T. H. Dupree, Phys. Fluids **15**, 334 (1972).
[8] J. C. Adam, G. Laval, and D. Pesme, in *Proceedings of the 1980 International Conference on Plasma Physics,* Nagoya, Japan (Fusion Research Association of Japan, Nagoya, 1980), p. 298.
[9] K. Theilhaber, G. Laval, and D. Pesme, Phys. Fluids **30**, 3129 (1987).
[10] W. E. Drummond and D. Pines, Ann. Phys. (N.Y.) **28**, 478 (1964); R. E. Aamodt and W. E. Drummond, Phys. Fluids **7**, 1816 (1964).
[11] J. R. Pierce, *Traveling Wave Tubes* (Van Nostrand, New York, 1950).
[12] W. E. Drummond, Phys. Fluids **7**, 816 (1964).
[13] S. I. Tsunoda and J. H. Malmberg, Phys. Fluids **27**, 2557 (1984).
[14] R. Z. Sagdeev and A. A. Galeev, *Nonlinear Plasma Theory* (Benjamin, New York, 1969).
[15] P. K. Tien, L. R. Walker, and V. M. Wolontis, Proc. IRE **43**, 260 (1955).
[16] G. M. Branch and T. G. Mihran, IRE Trans. Electron Devices **ED-2**, 3 (1955).
[17] T. M. O'Neil and J. H. Winfrey, Phys. Fluids **15**, 1514 (1972).
[18] A. Nordsieck, Proc. IRE **41**, 630 (1953).
[19] G. Dimonte and J. H. Malmberg, Phys. Fluids **21**, 1188 (1978).
[20] J. H. Malmberg, T. H. Jensen, and T. M. O'Neill, in *Plasma Physics and Controlled Nuclear Fusion Research* (IAEA, Vienna, 1966), Vol. I, p. 683.
[21] J. H. Malmberg and C. B. Wharton, Phys. Rev. Lett. **17**, 175 (1966).
[22] S. I. Tsunoda and J. H. Malmberg, Rev. Sci. Instrum. **57**, 2348 (1986).
[23] In any real system, of course, the spatial resolution would be determined by the probe geometry and by the proximity of the probe to the slow wave structure. In our experiment the resolution is roughly ~ 1 cm.
[24] The width of the plateau is ultimately limited in the following way: At large energies the number of particles is cut off at the maximum beam energy. At low energies the beam couples to the waves very poorly.
[25] T. M. O'Neil and J. H. Malmberg, Phys. Fluids **11**, 1754 (1968).
[26] The frequency spacing between neighboring modes is sufficiently narrow to ensure the overlap of resonances in phase space.
[27] W. L. Kruer, J. M. Dawson, and R. N. Sudan, Phys. Rev. Lett. **23**, 838 (1969).